First-Principles Study of Thermoelectric Properties of Half-Heusler Alloy $FeV_{1-x}Mn_xSb$ ($x = 0, 0.25, 0.5, 0.75$ and 1)

A. Azhar[a,*] and A.M.R. Dharmayanti[b]

[a] *Physics Study Program, Faculty of Science and Technology, Syarif Hidayatullah State Islamic University Jakarta, Ir H. Juanda Street No. 95, 15422, Tangerang Selatan, Indonesia*
[b] *Department of Physics, Faculty of Mathematics and Natural Sciences, University of Indonesia, Margonda Raya Street, 16424, Depok, Indonesia*

Received: 16.01.2022 & Accepted: 07.04.2022

Doi: 10.12693/APhysPolA.141.597 *e-mail: anugrahazhar@uinjkt.ac.id

The theoretical study of the thermoelectric properties of the $FeV_{1-x}Mn_xSb$ half-Heusler alloy ($x = 0$, 0.25, 0.5, 0.75, and 1) has been conducted using density functional theory. The aim of this research was to investigate the effect of Mn substitution on the FeVSb system in order to achieve a higher value of ZT. Our findings show that a system with an Mn doping concentration of $x = 0.75$ achieves the highest values of $ZT \sim 0.90$ for the spin-down states in the temperature range from 300 to 800 K, making it a promising candidate for future thermoelectric applications. On the other hand, the Mn substitution also triggers the magnetic moment formation and causes a large spin polarization at the Fermi level, leading the system to change from insulator to half-metallic.

topics: figure of merit, Heusler alloy, Seebeck coefficient, thermoelectric

1. Introduction

During operation, machines and electronic devices will generate heat. The heat they produce will then be wasted on the environment [1]. To take advantage of this condition, researchers studied thermoelectric materials (TM) that can directly convert heat into electricity [2]. The effectiveness of TM in a thermoelectric system is determined by several factors: electrical conductivity (σ), thermal conductivity (κ), and the Seebeck coefficient (S) [3]. Therefore, TMs are widely used in refrigerators and power generators in order to increase the efficiency of this electrical equipment [4, 5]. A beneficial TM is indicated by a high ZT value obtained with the formula

$$ZT = \frac{\sigma S^2}{\kappa_e + \kappa_L} T, \tag{1}$$

where T is the temperature. A high value of ZT can be achieved when a system has a high value of S and σ, and a low κ ($\kappa = \kappa_e + \kappa_L$). In (1), κ_e and κ_L refer to the thermal conductivity contributed by electrons and phonons, respectively.

Heusler alloys (HA) are considered to be one of the most promising candidates for TM. Changing the chemical formula of this material may readily modify its characteristics [6]. HA, due to their high tunability, have been extensively studied in a variety of fields, including shape memory materials [7], spintronics [8], superconductors [9], and thermoelectric (TE) devices [10]. In addition, due to their high ZT value of 1 and increasing to 1.5, half-Heusler (HH) alloys — one of the Heusler alloys families — have been extensively studied as any minor increase possibly results in numerous new applications [11–13]. Many Heusler alloys have half-metallic behaviour with a high spin polarized at the Fermi level. According to Chen et al. [14], sharp characteristics of the density of states around the Fermi energy (E_F) were identified in both MNiSn (n-type) and MCoSb (p-type) based HH that impact the Seebeck coefficient at room temperature.

In this paper, we investigate the impact of Mn substitution on the iron-based HH FeVSb to raise the S and ZT values of FeVSb. Since determining the thermal characteristics supplied by phonon, κ_L, involves a costly computation, we only examine the contribution of ZT by electron, i.e., ZT_e. It is illustrated as

$$ZT_e = \frac{\sigma S^2}{\kappa_e} T. \tag{2}$$

2. Computational method

First of all, the $FeV_{1-x}Mn_xSb$ model ($x = 0$, 0.25, 0.5, 0.75 and 1) was constructed using the BURAI software as a graphical user interface (GUI). The crystal structure of FeVSb can be seen in Fig. 1,

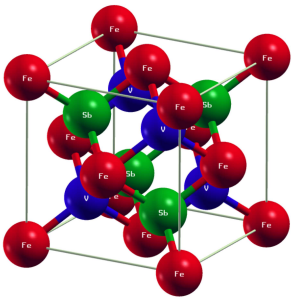

Fig. 1. Crystal structure of FeVSb where the Wyckoff position of Fe (red), V (blue), and Sb (green) are $(0,0,0)$, $(1/4,1/4,1/4)$, and $(3/4,3/4,3/4)$, respectively.

TABLE I

Lattice constant of $FeV_{1-x}Mn_xSb$ (x = 0, 0.25, 0.5, 0.75, and 1).

x	Lattice constant [Å]
0	5.7895
0.25	5.8009
0.5	5.8249
0.75	5.8267
1	5.8478

where the position of the V atom will then be replaced by the Mn atom. After building the model, Quantum-Espresso (QE) calculation was performed to obtain the density of states (DOS) and Fermi energy (E_F) of the system [15, 16]. The Perdew–Burke–Ernzerhof (PBE) exchange-correlation was used as the pseudopotential with a cut-off energy of 75 Ry and a cut-off charge density of 645 Ry. We also implement message passing interface (MPI) in order to reduce computational time [17].

Calculation of the variable cell relaxation (vc-relax) was applied to obtain the atomic positions and cell parameters of the material using $6\times6\times6$ k-points. The lattice constants of the material used in the calculation are shown in Table I. Then we performed the self-consistence field (SCF) calculation with $6\times6\times6$ k-points and non-self-consistence field (NSCF) calculation with $24\times24\times24$ k-points. For the measurements of thermoelectric properties, we performed Boltzmann transport calculations using the BoltzTraP package [18].

3. Results and discussions

3.1. Density of states and magnetic moment

The DOS for both spin states (spin-up and spin-down) is shown in Fig. 2, with E_F represented by a dashed green line. For $x = 0.00$, the DOS exhibits insulating behaviour for both spin states, and E_F lies on the edge of the valance band, indicating a p-type semiconductor.

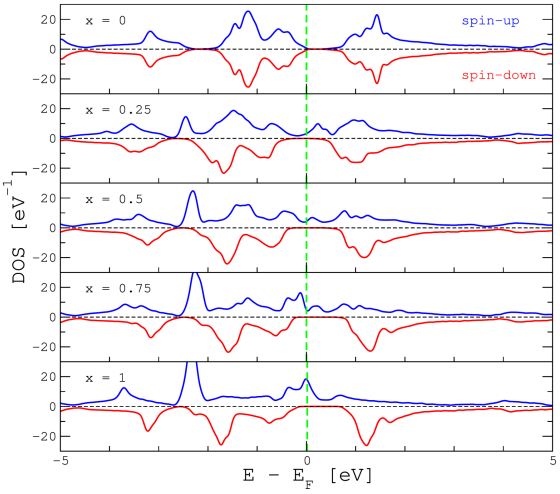

Fig. 2. The density of states for $FeV_{1-x}Mn_xSb$ with the blue line representing the spin-up states and the red line representing the spin-down states. For convenience, energy in horizontal axis is shifted by E_F.

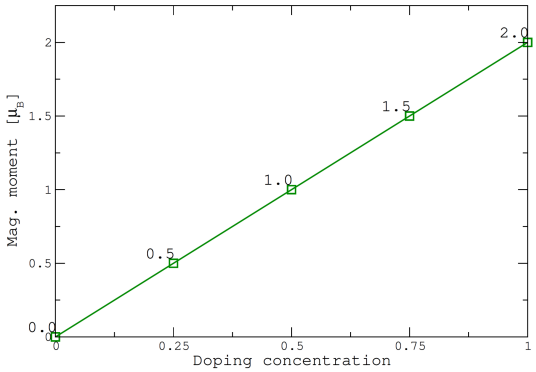

Fig. 3. The $FeV_{1-x}Mn_xSb$ magnetic moment [μ_B] (measured in Bohr magneton) as a function of the doping concentration.

On the other hand, for $x \geq 0.25$, the DOS of the spin-up (spin-down) states shows metallic (insulating) behaviour, making the system a half-metal. Sharma et al. [19] report a similar half-metal trend in the full-Heusler Co_2MnGe system. Romaka et al. [20] also report that $TiCo_{1-x}Ni_xSb$ shows the metal–insulator transition. This phenomenon appears due to a change in composition. One can deduce that strong ferromagnetism in the case of our HH will be brought by the atom Mn [21]. As a result, as the Mn doping concentration increases, the value of the magnetic moment of the system will increase, as shown in Fig. 3. The average value of local magnetic moment of each atom is given Table II.

3.2. Electrical and thermal conductivity

From the electrical conductivity data shown in Fig. 4, for a given temperature range, the highest value of σ/τ in the spin-up states occurs

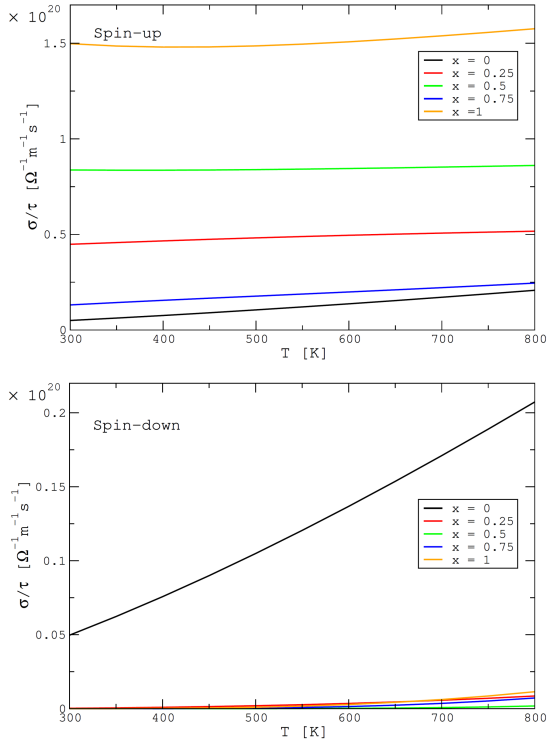

Fig. 4. Electrical conductivity (σ/τ) of $FeV_{1-x}Mn_xSb$ (x = 0, 0.25, 0.5, 0.75, and 1). The relaxation time τ can then be taken to be constant, around 10^{-14}, as is often assumed in BoltzTraP code [23].

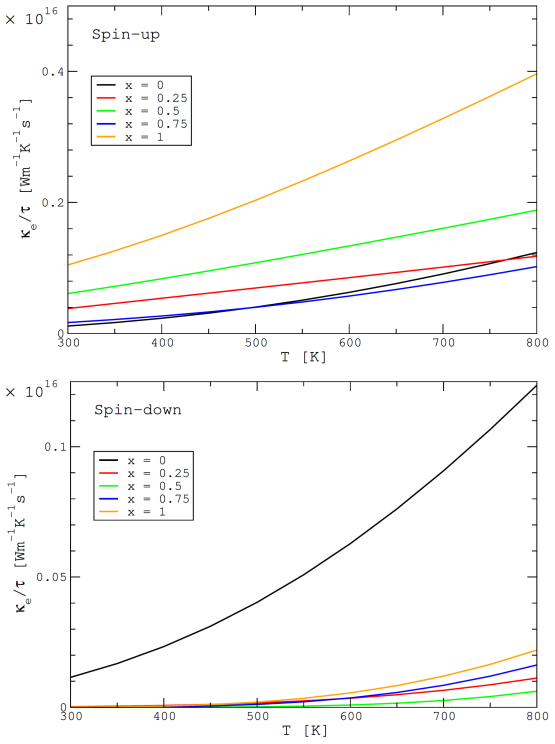

Fig. 5. Electron thermal conductivity (κ_e/τ) of $FeV_{1-x}Mn_xSb$ (x = 0, 0.25, 0.5, 0.75, and 1) for both spin-up and spin-down measured in the 300–800 K range.

TABLE II

Average value of local magnetic moment.

Compound	Magnetic moment [μ_B]			
	Fe	V	Mn	Sb
FeVSb	0.0	0.0	–	0.0
$FeV_{0.75}Mn_{0.25}Sb$	−0.46	0.19	0.73	−0.01
$FeV_{0.5}Mn_{0.5}Sb$	0.15	−0.70	1.51	−0.01
$FeV_{0.25}Mn_{0.75}Sb$	−0.83	0.06	2.25	−0.02
FeMnSb	−1.10	–	3.05	−0.01

for FeMnSb (about 1.5×10^{20} $(\Omega\ \mathrm{m\ s})^{-1}$), and then for $FeV_{0.5}Mn_{0.5}Sb$ ($\sim 0.7 \times 10^{20}$ $(\Omega\ \mathrm{m\ s})^{-1}$) and $FeV_{0.75}Mn_{0.25}Sb$ ($\sim 0.4 \times 10^{20}$ $(\Omega\ \mathrm{m\ s})^{-1}$). Meanwhile, in the studied temperature range, $FeV_{0.25}Mn_{0.75}Sb$ and FeVSb have very small $\sigma \approx 0.3 \times 10^{20}$ $(\Omega\ \mathrm{m\ s})^{-1}$. The value of σ changes depending on the relationship between Fe and Mn in materials [22]. The relaxation time τ in our calculation can then be taken as a constant value of $\simeq 10^{-14}$ [23].

In the spin-down cases, it should come as no surprise that a system with $x = 0$ has very high σ/τ values due to its insulating behaviour, and at $T = 0$ the conductivity goes to zero. For $x \geq 0.25$, systems exhibit insulating behaviour, as seen in Fig. 2, resulting in smaller σ/τ values.

Half-Heusler materials are known to have a low thermal conductivity which is suitable for high-efficiency thermoelectric materials [24]. The thermal conductivity contributed by electrons (κ_e/τ), for both spin-up and spin-down directions, is shown in Fig. 5. In spin-up cases, the highest value of κ_e/τ is given by FeMnSb, followed by $FeV_{0.5}Mn_{0.5}Sb$ and $FeV_{0.25}Mn_{0.75}Sb$, in that order, while FeVSb and $FeV_{0.25}Mn_{0.75}Sb$ show low κ_e values. However, when it comes to spin-down, FeVSb has extremely high thermal conductivity values compared to a system with an Mn-doping concentration of $x \geq 0.25$, indicating that FeVSb has good thermal conduction.

3.3. Seebeck coefficient and figure of merit

The Seebeck coefficient (S) of $FeV_{1-x}Mn_xSb$ is shown in Fig. 6. In the spin-up states, FeVSb exhibits exceptionally high S values compared to other doping concentration values. This occurs because E_F is close to the band edge of the DOS, as seen in Fig. 2. On the other hand, the situation is substantially different in the spin-down states. Systems with $x = 0.5$, $x = 0.75$, and $x = 1$ have higher values of S than systems with $x = 0$ and $x = 0.25$. A high S value in the materials with a high Mn content indicates the elimination of the bipolar effect in the alloy materials [25].

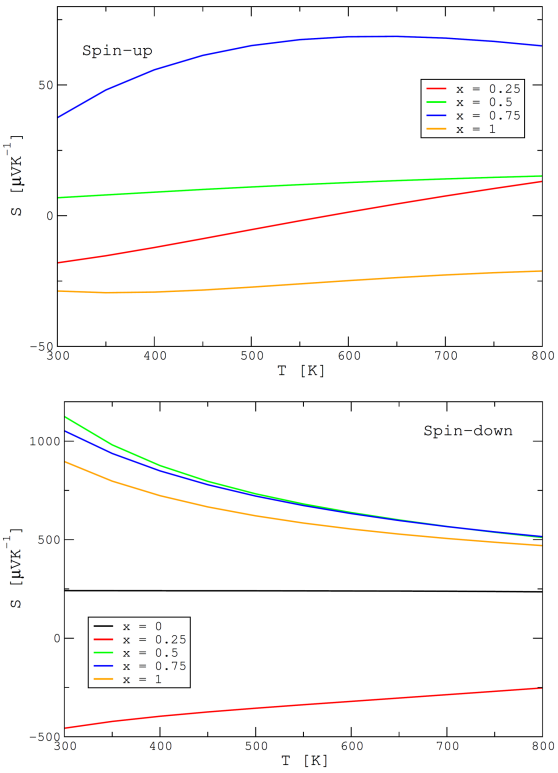

Fig. 6. Seebeck coefficient calculation of $FeV_{1-x}Mn_xSb$ (x = 0, 0.25, 0.5, 0.75, and 1) at many specific temperatures.

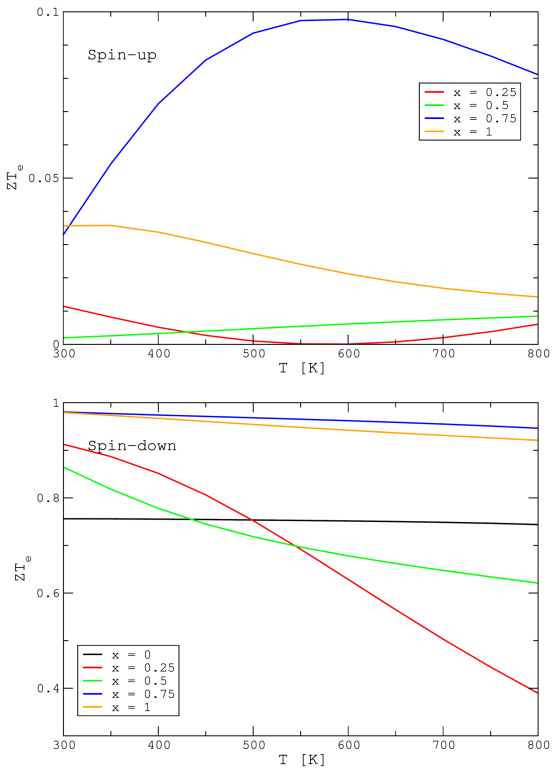

Fig. 7. Figure of merit of $FeV_{1-x}Mn_xSb$ (x = 0, 0.25, 0.5, 0.75, and 1) as a function of the temperature.

In the spin-up case, the majority of the charge carrier at $x = 0.5$ and $x = 0.75$ was contributed by positive charges (holes). In contrast, at $x = 1$, the majority of the charge carrier was contributed by negative charges (electrons). At $x = 0.25$, the majority of the charge carrier happened to be changed from negative to positive as the temperature increased. In the spin-down case, the majority of the charge carrier at all x values was contributed by the holes, except for $x = 0.25$, which lined up at the negative y-axis, indicating the contribution of electrons in its charge carrier. Therefore, in general, the increase in the concentration of Mn affects the increase in the charge carrier [26].

The electronic figure of merit (ZT_e) of $FeV_{1-x}Mn_xSb$ is shown in Fig. 7. FeVSb has the highest ZT_e value in the spin-up state compared to the Mn doped systems, which is consistent with the high S values of FeVSb. FeVSb performs well as a thermoelectric material in the spin-up states, however, the situation is drastically different in the spin-down cases. There, $FeV_{0.25}Mn_{0.75}Sb$ has the highest ZT_e value (about 0.9) for a given temperature range, followed by FeMnSb with slightly lower ZT_e values. Meanwhile, FeVSb has a moderate ZT_e of ≈ 0.75, whereas $FeV_{0.5}Mn_{0.5}Sb$ and $FeV_{0.75}Mn_{0.25}Sb$ have a diminishing ZT_e as the temperature rises.

4. Conclusions

We have studied the electronic and thermoelectric properties of $FeV_{1-x}Mn_xSb$ (x = 0, 0.25, 0.5, 0.75 and 1). Our results show that at a doping concentration of $x = 0.75$, the spin-down channel gives a high value of ZT_e around $\sim$ 0.9 in the temperature range of 300–800 K. The additional Mn also causes large spin polarization at the Fermi level and switches the system from insulating into the half-metal. The latter is indicated by the spin-up states behaving as in the case of metal, while the former by the spin-down states behaving as in the case of insulator. The results make $FeV_{1-x}Mn_xSb$ a good candidate for a thermoelectric material in terms of generated power.

Acknowledgments

The computation in this work has been done using the facilities of HPC BRIN, National Research and Innovation Agency (BRIN). We also acknowledge the financial support from UIN Syarif Hidayatullah Jakarta through BLU Research Grant No. B-208/LP2MPUSLITPEN/TL.03/08/2021.

References

[1] L. Miró, Sarah Bröckner, L.F. Cabeza, *Energy Rev.* **51**, 847 (2015).

[2] T. Kyono, R.O. Suzuki, K. Ono, *IEEE Power Eng. Rev.* **22**, 58 (2002).

[3] B. Hinterleitner, I. Knapp, M. Poneder et al., *Nature* **576**, 85 (2019).

[4] Chih Wu, *Appl. Therm. Eng.* **16**, 63 (1996).

[5] A.Z. Sahin, B.S. Yilbas, *Energy Convers. Manag.* **65**, 26 (2013).

[6] L. Wollmann, A.K. Nayak, S.S.P. Parkin, C. Felser, *Annu. Rev. Mater. Res.* **47**, 247 (2017).

[7] H. Abbassa, S. Meskine, A. Labdelli, S. Kacher, T. Belaroussi, B. Amrani, *Mater. Chem. Phys.* **256**, 123735 (2020).

[8] T. Graf, C. Felser, S.S.P. Parkin, in: *Heusler Compounds: Applications in Spintronics*, Springer, Dordrecht (Netherlands) 2016, p. 335.

[9] A.A. Kamashev, P.V. Leksin, N.N. Garif'yanov, A.A. Validov, J. Schumann, V. Kataev, B. Büchner, I.A. Garifullin, *J. Magn. Magn. Mater.* **459**, 7 (2018).

[10] T.M. Tritt, *Annu. Rev. Mater. Res.* **41**, 433 (2011).

[11] G.D. Mahan, J.O. Sofo, *Proc. Natl. Acad. Sci. U.S.A.* **93**, 7436 (1996).

[12] S.J. Poon, *J. Phys. D* **52**, 493001 (2019).

[13] F. Casper, T. Graf, S. Chadov, B. Balke, C. Felser, *Semicond. Sci. Technol.* **27**, 063001 (2012).

[14] Shuo Chen, Zhifeng Ren, *Mater. Today* **16**, 387 (2013).

[15] P. Giannozzi, S. Baroni, N. Bonini et al., *J. Phys.: Condens. Matter* **21**, 395502 (2009).

[16] P. Giannozzi, O. Baseggio, P. Bonfá et al., *J. Chem. Phys.* **152**, 154105 (2020).

[17] B. Schmidt, J. González-Domínguez, C. Hundt, M. Schlarb, in: *Parallel Programming*, Morgan Kaufmann, 2018, p. 315.

[18] G.K.H. Madsen D.J. Singh, *Comput. Phys. Commun.* **175**, 67 (2006).

[19] S. Sharma, S.K. Pandey, *J. Phys.: Condens. Matter* **26**, 215501 (2014).

[20] L.P. Romaka, M.G. Shelyapina, Yu.V. Stadnyk, D. Fruchart, E.K. Hlil, V.A. Romaka, *J. Alloys Compd.* **416**, 46 (2006).

[21] Bei Gao, Can Huang, Feng Zhu, Chun-Lan Ma, Yan Zhu, *Phys. Lett. A* **414**, 127636 (2021).

[22] J. Heo, G. Laurita, S. Muir, M.A. Subramanian, D.A. Keszler, *Chem. Mater.* **26**, 2047 (2014).

[23] J.P. Perdew, K. Burke, M. Ernzerhof, *Phys. Rev. Lett.* **77**, 3865 (1996).

[24] T.M Tritt, *Thermal Conductivity: Theory, Properties, and Applications*, Springer Science & Business Media, 2005.

[25] Qiang Sun, Zhi-Yu Chen, Meng Li et al., *Small* **17**, 2100525 (2021).

[26] Haixu Qin, Jianbo Zhu, Bo Cui et al., *ACS Appl. Mater. Interfaces* **12**, 945 (2020).